Bioimaging 1 (1993) 47–61. Printed in the UK

Estimators of 2D edge length and position, 3D surface area and position in sampled grey-valued images

Piet W Verbeek† and Lucas J van Vliet‡

Pattern Recognition Group of the Faculty of Applied Physics, Delft University of Technology, Lorentzweg 1, 2628 CJ Delft, The Netherlands

Received 21 October 1992

Abstract. Existing estimators for edge length in 2D and surface area in 3D are applied to a binary representation of the object. In this paper we estimate length and surface area through grey-volume measurements. Volume is measured without thresholding and does not introduce a sampling error. Object boundaries are carefully transformed into volumes using bandlimited operations.

We give two methods: GC and GCL. The GC method measures the length of an isophote. The GCL method measures the length of the Laplacian zerocrossing line. The GC estimator is biased because the isophote position is shifted towards smaller radii due to both analogue and digital low-pass filtering. The GCL estimator contains a compensating mechanism and yields unbiased results for both the edge position and the length.

Extension of both methods to 3D images is straightforward. The 3D GC area bias is scale independent. The 3D GCL method yields unbiased edge position. For 3D objects without tunnels or enclosed cavities the 3D GCL area bias amounts to a constant correction per object and an unbiased estimator can still be constructed.

Keywords: edge position, edge length, surface area, Laplace, second derivative in gradient direction, edge bias, low-pass filters, curved edge location, measurement accuracy and precision, derivatives of Gaussian.

1. Introduction

The estimation of edge length such as the perimeter of an object from its digital image is a well-known problem in biomedical image analysis. There exists an extensive literature that describes techniques for measuring length given a 2D binary representation. We can distinguish algorithms designed and optimized for digital straight lines and algorithms designed for measuring the arc length of an arbitrary curve or contour.

Since Freeman (1970) introduced chain coding of 2D lines, people have investigated length estimators based on this representation. Techniques suitable for straight lines were proposed by Proffitt and Rosen (1979), Vossepoel and Smeulders (1982), Dorst (1986), Dorst and Smeulders (1986, 1987). An overview is given by Dorst and Smeulders (1987). Estimators for arc length of digitized curved lines and contours were proposed by Kulpa (1977), Groen and Verbeek (1978), Ellis and Proffitt (1979), Dorst and Smeulders (1987). Young (1988) summarizes experimental results for the corner count method (Vossepoel and Smeulders 1982) and validates Groen's conjecture that this technique, originally optimized for straight lines, produces a constant bias term when applied to circles. A common factor of the above mentioned algorithms is that pixels along a line segment are classified into a limited number of classes (e.g. local direction: horizontal/vertical or diagonal) and weighted by a set of coefficients that optimize a certain error criterion. The sum of weighted pixels is the length estimate. Note that the ordering, used to build a string of chain codes and to classify the arc-pixels, is not used any further. A recent article by Eberly and Lancaster (1991) claims to measure the arc length directly from the grey-scale image. Close examination shows that their approach is similar to the chain code based techniques. Instead of classifying the arc-pixels they are weighted by a factor derived from the underlying grey-scales.

Arc length in 2D is analogous to surface area in 3D. Eberly *et al* (1991) showed that his algorithm can also

† E-mail address: piet@ph.tn.tudelft.nl
‡ E-mail address: lucas@ph.tn.tudelft.nl

0964-1726/93/010047+15$07.50

measure surface area in 3D. Mullikin and Verbeek (1993) extended the binary technique to three dimensions. Although this algorithm is optimized for planes it produces a constant bias term when measuring closed surfaces. Other techniques to estimate the surface area come mainly from stereology (Hahn and Sandau 1989, Gesbert *et al* 1990, Howard and Sandau 1992, Meyer 1992).

Practical recipes have been proposed to estimate edge length in 2D (Young 1988) and surface area in 3D (Mullikin and Verbeek 1993) for the worst case in which only a binary image is available. Fitting an analytical curve to interpolated digital contour points and calculating its length is a more theoretically founded approach (Mullikin 1992).

We believe that in the thresholding that usually produces the binary image valuable information is lost that should be preserved to improve the estimation of edge length.

The method presented here works on grey value images and combines edge detection (2D and 3D) and edge length (in 2D)/surface area (in 3D) estimation. Apart from a few plausible assumptions it is founded on sampling theory.

Section 2 gives the relation between analogue and sampled images on which the method is based. Sections 3 and 4 remain in the analogue domain. Section 5 discusses the means to salvage the analogue information from sampled images. Section 6 deals with a systematic error and section 7 gives the means to compensate for it. Section 8 shows how to extend from 2D to 3D. Section 9 discusses the various methods and strategies, e.g. GC and GCL. Section 10 gives an experimental evaluation.

2. Analogue information from samples

Edge detection is generally based on thresholding. The simplest example is thresholding of the original grey image at a fixed level, e.g. half edge height. Thresholding the original image at a space-variant level (a reference image that can be derived from the original by low-pass filtering or local minimum and maximum filtering (Verbeek *et al* 1988)) is equivalent to high-pass filtering and thresholding at a fixed level. In particular, one often thresholds a second derivative at level zero. This introduces noise sensitivity but solves the level selection problem.

Thresholding is a very nonlinear operation in the sense that the Taylor series expansion of the corresponding scaling function—threshold (*grey level*) $\rightarrow \{0, 1\}$—has appreciable higher-order terms. Consequently, thresholding in the continuous domain can only be replaced by an equivalent digital operation 'sampling $\rightarrow$ digital thresholding $\rightarrow$ interpolation' at the cost of equally appreciable oversampling (Verbeek 1985).

Direct estimation of the edge length or surface area in the discrete domain is a problem, grey-volume estimation is not.

Theorem. The volume of a grey value landscape (integrated grey value) is directly proportional to the sum of the samples if only the Nyquist criterion is fulfilled. In fact, only the DC component of the spectrum is used; this allows undersampling by a factor of two.

Proof. For each bandlimited image $h(x, y)$ with Fourier transform $(\tilde{h}(u, v)$ sampled at intervals Δ_x and Δ_y the following holds if $\tilde{h}(0, 0)$ is not corrupted due to aliasing.

$$\begin{aligned}
\text{volumeof}(h(x, y)) &= \Delta_x \Delta_y \sum_{i,y} h(i\Delta_x . j\Delta_y) \\
&= \iint h(x, y) \Delta_x \Delta_y \sum_{i,j} \delta(x - i\Delta_x)\delta(j - i\Delta_y)\, dx\, dy \\
&= \left[\tilde{h}(u, v) * (2\pi)^2 \sum_{k,l} \delta\left(u - k\frac{2\pi}{\Delta_x}\right)\delta\left(v - l\frac{2\pi}{\Delta_y}\right) \right]_{u=v=0} \\
&= (2\pi)^2 \tilde{h}(0, 0) = \iint h(x, y)\, dx\, dy \qquad (1)
\end{aligned}$$

with

$$\frac{2\pi}{\Delta_x} > u_{\max} \quad \text{and} \quad \frac{2\pi}{\Delta_y} > v_{\max}$$

where $u_{\max}$ and $v_{\max}$ are the highest frequencies of $h(x, y)$ in the x- and y-direction respectively. Sampling at Nyquist rate (twice the highest frequency) preserves the entire spectrum. Undersampling by a factor of two (sampling at the highest frequency) only preserves the zero frequency.

This has led us to look for an estimation method where edge length is expressed in a volume measure.

3. Edge length as volume

3.1. Straight edges

To start with, we employ our argument in the continuous domain. In order to convert an edge length into a volume of a grey value landscape proportional to it we can see from dimension considerations that we must multiply by a constant width and a constant height. For an edge of constant grey level (constant edge range) this value can be used as constant height. But the problem remains how to introduce a constant width.

The solution we found is to apply an *analogue isotropic local maximum filter* of diameter *fsize* to the analogue edge. The effect of which is mainly a sideways translation of the edge over the filter radius.

The volume enclosed between the original and the translated edge is then equal to

$$\text{volumeof(max} - \text{ori)} = \text{length} \cdot \text{fsize}/2 \cdot \text{edgeheight} \quad (2)$$

with max being the result after maximum filtering and ori the original edge image.

For a straight edge the relation is exact as long as the maximum filtering truly amounts to translation. We shall discuss ways to ensure this.

3.2. Curved edges

For a curved edge, maximum filtering will not only translate the edge, but will also change the edge radius. From the simple example of a circular step edge we see that it is then better to apply two filters, an analogue round local maximum filter and an analogue round local minimum filter, to the original edge. The volume enclosed between the results is then equal to

$$\text{volumeof(max} - \text{min)} = \text{length} \cdot \text{fsize} \cdot \text{edgeheight}. \quad (3)$$

For an edge of different shape it is more complicated to define edge position and edge length. There are several traditional definitions of edge position. The simplest is based on thresholding which produces a binary edge. In section 7 we show how edge length according to other traditional definitions—such as the zero crossing of a second derivative—can be handled. For now, we remark that (3) holds for one particular uncommon definition of edge position (cf figure 1): the average (continuous) position r_{eff} of the binary edge in a cross section perpendicular to the edge, when the average is taken over the entire interval of threshold levels (0, edgeheight).

This follows immediately from the expression below for a sector $d\varphi$ of the enclosed volume

$$\begin{aligned}\frac{\partial \text{volumeof(max} - \text{min)}}{\partial \varphi} &= \int_0^{\text{edgeheight}} \int_{r(h)-(\text{fsize}/2)}^{r(h)+(\text{fsize}/2)} r \, dr \, dh \\ &= \frac{1}{2} \int_0^{\text{edgeheight}} \\ &\times [(r(h) + \text{fsize}/2)^2 - (r(h) - \text{fsize}/2)^2] \, dh \\ &= \text{fsize} \int_0^{\text{edgeheight}} r(h) \, dh \equiv \text{fsize} \cdot \text{edgeheight} \cdot r_{\text{eff}}.\end{aligned} \quad (4)$$

4. Isophote edge length

In practice the edge height will show ripple and noise. To achieve a simulated constant height we apply clipping at two levels clip_{low} and $\text{clip}_{\text{high}}$. This amounts to using a more general definition of edge position (cf figure 2): the average (continuous) position r_{eff} of the binary edge in a cross section perpendicular to the edge, when the average is taken within a range of 'threshold' levels (clip_{low},$\text{clip}_{\text{high}}$).

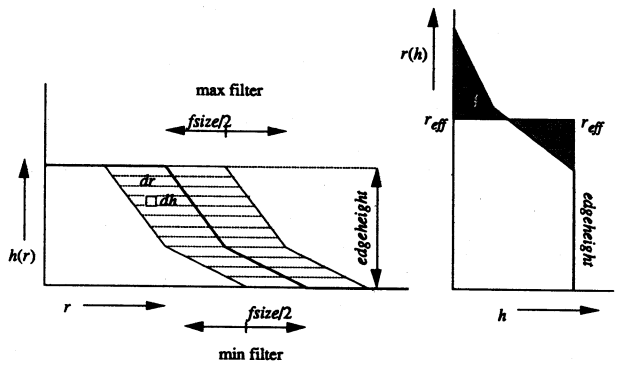

Figure 1. Cross section perpendicular to an edge of constant height.

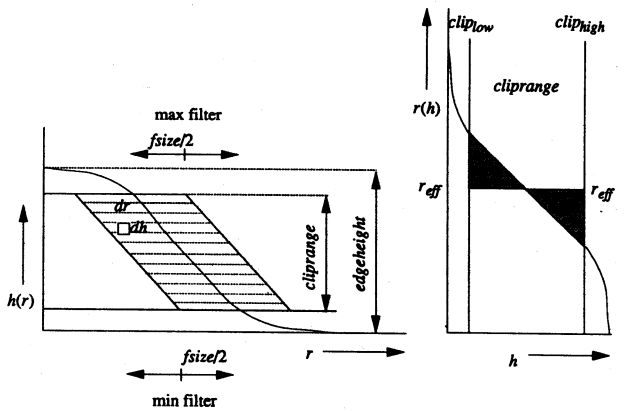

Figure 2. Cross section perpendicular to the edge; r_{eff} is the average position of the binary edge, when the average is taken over an interval of threshold levels (clip_{low},$\text{clip}_{\text{high}}$).

In particular, the clipping levels can be chosen close together around a fixed pseudo-threshold level t. Then the length calculated is that of the isophote at level t. As we are still handling continuous positions we have constructed a continuous analogy to contour length. Just like discrete contour length, our edge length depends on a 'threshold' level.

5. Continuous edge length from a sampled image

When assessing the volume that is representative for edge length it makes little difference whether the image is sampled or not. For a properly sampled bandlimited image the integral over continuous grey value is directly proportional to the sum of the grey value samples.

Two operations used to convert edge length into

volume need attention when assessing continuous contour length from a sampled image:

(a) the analogue maximum filter used for translation of the edge must be replaced by a discrete operation which on the basis of the sampled image yields the sample values of the translated continuous edge;
(b) the clipping operation being a nonlinear scaling function must be handled with care.

In both issues an approximation is proposed to make a practical compromise between bandlimitation and accuracy.

5.1. Isotropic analogue maximum and minimum filters

Translation of a 1D edge profile (cf figure 1) over fsize/2 is approximated by a truncated Taylor series expansion.

$$h(r + \text{fsize}/2) = h(r) + (\text{fsize}/2)\frac{\partial h(r)}{\partial r} + \tfrac{1}{2}(\text{fsize}/2)^2 \frac{\partial^2 h(r)}{\partial r^2}. \tag{5}$$

In D-dimensional space with r along the gradient direction (here $D = 2$) we obtain translations equivalent to the isotropic local maximum and local minimum filters

$$h\left(r + \frac{\text{fsize}}{2}\right) = h(x, y) + \left(\frac{\text{fsize}}{2}\right)|\text{grad}(h(x, y))| + \frac{1}{2}\left(\frac{\text{fsize}}{2}\right)^2 \text{SDGD}(h(x, y)) \tag{6}$$

$$h\left(r - \frac{\text{fsize}}{2}\right) = h(x, y) - \left(\frac{\text{fsize}}{2}\right)|\text{grad}(h(x, y))| + \frac{1}{2}\left(\frac{\text{fsize}}{2}\right)^2 \text{SDGD}(h(x, y)) \tag{7}$$

where

$$\text{grad}(h(x, y)) = (\partial h/\partial x, \partial h/\partial y)$$

and SDGD stands for second derivative in the gradient direction and can be written as

$$\text{SDGD}(h) = \frac{\text{grad}(h) \cdot H(h) \cdot \text{grad}(h)}{|\text{grad}(h)|^2}$$

in which $H(h)$ is the Hessian matrix

$$H(h) = \begin{pmatrix} \partial^2 h/\partial x^2 & \partial^2 h/\partial x\, \partial y \\ \partial^2 h/\partial x\, \partial y & \partial^2 h/\partial y^2 \end{pmatrix}.$$

Although the derivatives are all bandlimited, the modulus of the gradient and the SDGD convert a bandlimited image into results that can only be hoped to be approximately bandlimited. The reason for this hope is in the fact that nonlinearity of the modulus and of the SDGD does hardly occur in the centre part of the edges which we select for edge length estimation.

5.2. Soft clipping curbs aliasing

Sampling theory cannot predict the errors in the analysis of thresholded images. We shall show that it can when a smooth clipping is applied instead of thresholding. Clipping a sampled image is equivalent to clipping the continuous image and sampling; clipping the continuous image distorts the grey value landscape so that it is no longer bandlimited. (The distortion is already much weaker than the one caused by thresholding.) In order to reduce aliasing we propose to replace the grey scaling function of clipping by a smoother function, the error function, between the same levels: 'erf clipping'.

$$\text{clip}_{\text{erf}}(h(r)) = t + \tfrac{1}{2}\text{cliprange} \cdot \text{erf}\left(\frac{\sqrt{\pi}}{\text{cliprange}}[h(r) - t]\right) \tag{8}$$

with $\text{cliprange} \equiv (\text{clip}_{\text{high}} - \text{clip}_{\text{low}})$ and pseudo-threshold level $t \equiv (\text{clip}_{\text{high}} + \text{clip}_{\text{low}})/2$. In cross sections where the edge slope between clipping levels is approximately constant, $h(r) = ar + b$, the edge is shaped into a scaled error function

$$\text{clip}_{\text{erf}}(h(r)) = t + \tfrac{1}{2}\text{cliprange} \cdot \text{erf}\left(\frac{\sqrt{\pi}}{\text{cliprange}}[ar + b - t]\right) \tag{9}$$

the approximate bandwidth of which is $f_{\text{max erf}}$ (lemma 1) limited by (lemma 2)

$$f_{\text{max erf}} = \max\left[\frac{2a}{\sqrt{2\pi}\text{cliprange}}\right] \approx \sqrt{2\pi}\frac{\text{edgeheight}}{\text{cliprange}} f_{\max}. \tag{10}$$

Hence, if the clipping interval and the linear part of the edge slope encompasses $1/k$ of the total grey range, the erf clipping theoretically needs $k\sqrt{2\pi}$ times oversampling.

For practical use we apply lemmas 3 and 4. For a step edge which is filtered with a Gaussian of width σ_{preclip} we get

$$f_{\text{max erf}} \approx \frac{1}{\pi\sigma_{\text{preclip}}}\frac{\text{edgeheight}}{\text{cliprange}}. \tag{11}$$

A practical choice for the cliprange is edgeheight/4. The desired $f_{\text{max erf}} \leqslant 1$ is obtained for

$$\sigma_{\text{preclip}} \geqslant 4/\pi \approx 1.27.$$

For the second derivative of a step edge which is filtered with a Gaussian of width σ_{preclip} we get (grey-scale

invariant)

$$f_{\max \mathrm{erf}} \approx \frac{\sqrt{e}}{\sqrt{2\pi}\sigma_{\mathrm{preclip}}} \frac{\mathrm{secderrange}}{\mathrm{cliprange}}. \quad (12)$$

A practical choice for the cliprange is secderrange/4. The desired

$$f_{\max \mathrm{erf}} \leqslant 1 \quad (13)$$

(undersampling by a factor 2 allowed for volume estimation, cf section 2) is obtained for

$$\sigma_{\mathrm{preclip}} \geqslant 4\sqrt{e}/\sqrt{2\pi} \approx 2.63.$$

Lemma 1. The approximate bandwidth of erf(cr) is $(c\sqrt{2})/\pi$.

Proof of lemma 1. As a signal and its derivative have the same bandwidth, we take for the approximate bandwidth $f_{\max \mathrm{erf}}$ of the error function the value of $2\sigma_{\mathrm{freq}} = 1/(\pi w)$ of the Gauss function with width w of which it is the integral.

As the error function is defined as $\mathrm{erf}(z) \equiv (2/\sqrt{\pi}) \int_0^z \exp(-\zeta^2)\,\mathrm{d}\zeta$, we have $\mathrm{erf}(cr) = (2/\sqrt{\pi})c \int_0^r \exp(-c^2\zeta^2)\,\mathrm{d}\zeta$, based on a Gaussian with variance $w^2 = 1/(2c^2)$. Thus, the approximate bandwidth is $f_{\max \mathrm{erf}} = 2\sigma_{\mathrm{freq}} = 1/(\pi w) = (c\sqrt{2})/\pi$. □

Lemma 2. The original slope is limited by $a \leqslant a_{\max} \equiv 2\pi f_{\max}\,\mathrm{greyrange}/2$ where $f_{\max}$ is the maximum frequency in the original cross section.

Proof of lemma 2. The steepest slope occurs if all allowed frequencies add up with the same phase

$$\frac{\partial}{\partial x} \int A(f) \sin(2\pi f x)\,\mathrm{d}f \Big|_{x=0} = 2\pi \int A(f) f\,\mathrm{d}f \quad (14)$$

the maximum signal value that can occur for given spectrum-amplitude $A(f)$ is

$$\int A(f) \cos(2\pi f x)\,\mathrm{d}f \Big|_{x=0} = \int A(f)\,\mathrm{d}f. \quad (15)$$

The spectrum that gives the steepest slope with respect to the maximum signal $h_{\max}$ = greyrange/2 has amplitude $A(f) = h_{\max}\delta(f - f_{\max})$, with steepest slope

$$a_{\max} = 2\pi f_{\max} h_{\max} = 2\pi f_{\max}\,\mathrm{greyrange}/2. \quad (16)$$

□

Lemma 3. If the original slope concerns a step edge which is filtered with a Gaussian of width $\sigma_{\mathrm{preclip}}$ then the slope is limited by $a \leqslant a_{\mathrm{maxGauss}} \equiv \mathrm{edgeheight}/(\sigma_{\mathrm{preclip}}\sqrt{2\pi})$.

Lemma 4. If the original slope concerns the second derivative of a step edge which is filtered with a Gaussian of width $\sigma_{\mathrm{preclip}}$ then the slope is limited by $a \leqslant a_{\mathrm{maxsecder}} \equiv \mathrm{edgeheight}/(\sigma_{\mathrm{preclip}}^3\sqrt{2\pi}) = \sqrt{e}/(2\sigma_{\mathrm{preclip}})$ secderrange, where secderrange is the difference between the maximum and minimum second derivative value.

Proof of lemmas 3 and 4. It is sufficient to consider a straight step edge of height edgeheight. Its derivative is edgeheight $\delta(x)$, which by Gaussian smoothing gives the slope of the smoothed edge

$$(\mathrm{edgeheight}/\sqrt{2\pi}\sigma_{\mathrm{preclip}}) \exp\left(-\frac{x^2}{2\sigma_{\mathrm{preclip}}^2}\right) \quad (17)$$

with maximum slope

$$a_{\mathrm{maxGauss}} \equiv \mathrm{edgeheight}/(\sqrt{2\pi}\sigma_{\mathrm{preclip}}). \quad (18)$$

The second derivative is

$$(-x \cdot \mathrm{edgeheight}/\sqrt{2\pi}\sigma_{\mathrm{preclip}}^3) \exp\left(-\frac{x^2}{2\sigma_{\mathrm{preclip}}^2}\right) \quad (19)$$

with slope

$$\mathrm{edgeheight}((1 - x^2/\sigma_{\mathrm{preclip}}^2)/\sqrt{2\pi}\sigma_{\mathrm{preclip}}^3) \times \exp\left(-\frac{x^2}{2\sigma_{\mathrm{preclip}}^2}\right) \quad (20)$$

and range

$$\mathrm{secderrange} \equiv 2e^{-1/2}\mathrm{edgeheight}/\sqrt{2\pi}\sigma_{\mathrm{preclip}}^2. \quad (21)$$

The maximum slope of the second derivative is

$$\mathrm{edgeheight}/\sqrt{2\pi}\sigma_{\mathrm{preclip}}^3 = \sqrt{e}\,\mathrm{secderrange}/2\sigma_{\mathrm{preclip}}. \quad (22)$$

□

6. Curved-edge displacement by Gaussian filters

Our new technique calculates the length of an isophote of the grey image. The derivative filters of section 5.1 are implemented as derivatives of a Gaussian. This is equivalent to calculating the length of the isophote in the grey image with pure derivatives after smoothing the grey image with the Gaussian. However, the Gaussian low-pass filter—like all low-pass filters—displaces a curved isophote towards the centre of curvature. We shall show that the displacement of an erf-clipped constant gradient edge caused by a Gaussian filter of size σ is $-\sigma^2/2R$. The displacement does not depend on the order in which clipping and shifting are performed. It always results in an edge length bias

$$\int_{\mathrm{object\ contours}} \frac{\sigma^2}{2R}\,\mathrm{d}\varphi. \quad (23)$$

The displacement of an erf-clipped constant gradient edge caused by a Gaussian filter of size σ can be calculated as follows.

For a constant-slope circular edge $h(r) = ar + b$ the erf-clipped result was given in (9)

$$\text{clip}_{\text{erf}}(h(r)) = t + \tfrac{1}{2}\text{cliprange} \times \text{erf}\left(\frac{\sqrt{\pi}}{\text{cliprange}}[ar + b - t]\right) \equiv h_{\text{clip}}(r) \qquad (24)$$

where $r^2 \equiv x^2 + y^2$. To study the impact of 2D smoothing it suffices to consider the result along the x-axis (radial behaviour).

Edge positions $r = R$ (e.g. $x = R$, $y = 0$) correspond to $ar + b - t = 0$. The unsmoothed |gradient| would be

$$\left|\frac{\mathrm{d}}{\mathrm{d}r} h_{\text{clip}}(r)\right| = a \exp\left(-\frac{(r-R)^2}{2w^2}\right) \qquad (25)$$

with clipwidth

$$w \equiv \text{cliprange}/(a\sqrt{2\pi}) = 1/(\pi f_{\max \text{erf}}). \qquad (25a)$$

We smooth by a normalized 2D Gaussian low-pass filter, split up in two 1D convolutions

$$\frac{1}{\sqrt{2\pi}\sigma}\exp\left(-\frac{x^2}{2\sigma^2}\right) * \frac{1}{\sqrt{2\pi}\sigma}\exp\left(-\frac{y^2}{2\sigma^2}\right) *.$$

First we perform the (tangential) y-smoothing. As the result on the x-axis is determined by the contributions from a strip of width $\approx 3\sigma$ along it and as we are interested in the edge postion $x \approx R$ we approximate $y \ll x$ and get

$$r \approx \sqrt{(x-R)^2 + (x-R)y^2/R}$$

and

$$\begin{aligned}\frac{1}{\sqrt{2\pi}\sigma}\exp\left(-\frac{y^2}{2\sigma^2}\right) * \left|\frac{\mathrm{d}}{\mathrm{d}r} h_{\text{clip}}(r)\right|_{y=0} &\approx a\exp\left(-\frac{(x-R)^2}{2w^2}\right) F_y\left(\frac{x-R}{R}\right) \\ &\approx a\exp\left(-\frac{(x-R+\sigma^2/2R)^2}{2w^2}\right) \qquad (26)\end{aligned}$$

for $x - R < 3w$ and $\sigma < 2\sqrt{wR}$ with

$$\begin{aligned}F_y\left(\frac{X}{R}\right) &\equiv \frac{1}{\sqrt{2\pi}\sigma}\exp\left(-\frac{y^2}{2\sigma^2}\right) * \exp\left(-\frac{y^2 X}{2w^2 R}\right)\Big|_{y=0} \\ &= \frac{1}{\sqrt{2\pi}\sigma}\int_{-\infty}^{\infty}\exp\left(-\frac{y^2}{2\sigma^2}\right)\exp\left(-\frac{y^2 X}{2w^2 R}\right)\mathrm{d}y \\ &= \left(1 + \frac{\sigma^2 X}{w^2 R}\right)^{-1/2} \approx \exp\left(-\frac{\sigma^2 X}{2w^2 R}\right)\end{aligned}$$

for $X/R \ll w^2/\sigma^2$.

Note that tangential smoothing displaces the edge by $-\sigma^2/2R$. This is in the direction of the osculating circle.

Next we perform the (radial) x-smoothing and get

$$\begin{aligned}\left|\frac{\mathrm{d}}{\mathrm{d}r} h_{\text{clip}}(r)\right|_{\text{smoothed}} &\approx \frac{1}{\sqrt{2\pi}\sigma}\exp\left(-\frac{x^2}{2\sigma^2}\right) * \\ &\quad \times a\exp\left(-\frac{(x - R + \sigma^2/2R)^2}{2w^2}\right)\Big|_{x=r} \\ &= \frac{aw}{\sqrt{\sigma^2 + w^2}}\exp\left(-\frac{(r - R + \sigma^2/2R)^2}{2(\sigma^2 + w^2)}\right) \qquad (27)\end{aligned}$$

for $\sigma < 2\sqrt{wR}$.

Note that radial smoothing broadens the edge and reduces the slope by a factor $w/\sqrt{\sigma^2 + w^2}$.

The Gaussian shape of $|\mathrm{d}/\mathrm{d}r\, h_{\text{clip}}(r)|$ and the erf character of $h_{\text{clip}}(r)$ are largely preserved by Gaussian smoothing.

7. Zerocrossing of Laplacian edge length

When edge height varies slowly as in shading, the length of an isophote does not represent edge length properly. The edge is then defined as the position where a second derivative of the edge crosses zero. Examples of second derivative filters are: the Laplacian, the second derivative in the gradient direction (SDGD) and their sum (PLUS) (Verbeek and van Vliet 1991). In earlier work we studied the location error for these operators on curved edges due to low-pass filtering (van Vliet and Verbeek 1991, Verbeek and van Vliet 1991) (see also Berzins 1984). Starting from the physical edge two types of low-pass filtering are common: optical (approximately Gaussian, width σ_{PSF}) and a Gaussian filter used in implementing the second derivative filter which at the same time suppresses noise (width σ_{secder}). Together they result in a Gaussian low-pass filtering of the physical edge (width σ_{preclip}). Table 1 summarizes the results for Gaussian low-pass filtered edges in 2D and 3D images.

Table 1. Theoretically derived (Verbeek and van Vliet 1991) relative location error of constant curvature edges as function of σ_{preclip} and the radius of osculating circle (sphere) at every edge location. The positive axis is defined from the centre of the osculating circle (sphere).

	2D	3D
SDGD	$-(0.29 \text{ to } 1.3)\left(\frac{\sigma_{\text{preclip}}}{R}\right)^2$	$-(0.5 \text{ to } 4.0)\left(\frac{\sigma_{\text{preclip}}}{R}\right)^2$
Laplace	$(0.45 \pm 30\%)\left(\frac{\sigma_{\text{preclip}}}{R}\right)^2$	$(0.83 \pm 20\%)\left(\frac{\sigma_{\text{preclip}}}{R}\right)^2$
PLUS	$(0.43 \pm 14\%)\left(\frac{\sigma_{\text{preclip}}}{R}\right)^4$	$(1.1 \pm 10\%)\left(\frac{\sigma_{\text{preclip}}}{R}\right)^4$

In (26) we calculated that, due to the smoothing (σ) in our gradient filters, the position of an isophote of a sloped edge is displaced towards the centre of the osculating circle. Taking $\sigma \approx \sigma_{\text{preclip}}$ the shift is of the same order but in opposite direction as the one caused by the Laplacian (of Gaussian, width σ_{Laplace}). Measuring the length of the zerocrossing (i.e. the zero-isophote) of the Laplacian (of Gaussian) then solves both the displacement problem and the shading problem (a practical application is shown in figure 4).

Note that

$$\sigma \approx \sigma_{\text{preclip}} \equiv \sqrt{\sigma_{\text{PSF}}^2 + \sigma_{\text{sec der}}^2} = \sqrt{\sigma_{\text{PSF}}^2 + \sigma_{\text{Laplace}}^2}.$$

Remark. Applying erf-clipping and Gaussian smoothing *without gradient* to the result of Laplacian-of-Gaussian edge detection will likewise correct the zerocrossing *position.*

8. Extension to 3D

The extension to 3D is rather straightforward. Some deviations from the 2D case are given below.

8.1. Isophote surface area

The main difference with our 2D edge length measurement is that our 3D surface area estimation is biased due to edge width.

In 3D a patch of surface is characterized by two curvatures in orthogonal directions, with radii R_1 and R_2 to be defined later. For each patch we define a local coordinate system with a coordinate r along grad h. As there are two radii we can no longer use the centre as the $r = 0$ reference. Instead we take the average of $r(h)$ over the grey range of the edge to be the $r = 0$ reference. (In 2D this characterized r_{eff}.) The radii R_1 and R_2 can now be defined as radii from two centres to the $r = 0$ position. Let the patch span an angle $\mathrm{d}\phi_1$ with radius R_1 and an angle $\mathrm{d}\phi_2$ with radius R_2, together a solid angle $\mathrm{d}\Omega = \mathrm{d}\phi_1\,\mathrm{d}\phi_2$ then the contribution of the patch to the estimated area is (following the max-min filter description of (4) of section 3.2)

$$\begin{aligned}
&\frac{\mathrm{d}\,\text{volumeof(max} - \text{min)}}{\text{fsize}\cdot\text{edgeheight}} \\
&\quad = \frac{1}{\text{fsize}\cdot\text{edgeheight}} \int_0^{\text{edgeheight}} \int_{r(h)-\text{fsize}/2}^{r(h)+\text{fsize}/2} \\
&\quad \times (R_1 + r)(R_2 + r)\,\mathrm{d}r\,\mathrm{d}h\,\mathrm{d}\Omega \\
&\quad = \frac{1}{\text{edgeheight}} \int_0^{\text{edgeheight}} \\
&\quad \times [R_1R_2 + \tfrac{1}{12}\text{fsize}^2 + (R_1 + R_2)r(h) + r^2(h)]\,\mathrm{d}h\,\mathrm{d}\Omega \\
&\quad = (R_1R_2 + \text{fsize}^2/12 + M_2)\,\mathrm{d}\Omega \qquad (28)
\end{aligned}$$

with second moment M_2

$$M_2 \equiv \frac{1}{\text{edgeheight}} \int_0^{\text{edgeheight}} r^2(h)\,\mathrm{d}h.$$

For fsize $\to 0$ and $r(h) = 0$ (step edge) we get $R_1R_2\,\mathrm{d}\Omega$ as the unbiased patch area. Hence the radii R_1 and R_2 of the average $r(h)$ surface are the effective radii. The term $\text{fsize}^2\,\mathrm{d}\Omega/12$ is the same for all patches. For each object without tunnels or enclosed cavities the solid angles $\mathrm{d}\Omega$ add up to 4π and the fsize-dependent term leads to a constant total-area bias of $\pi\text{fsize}^2/3$. The second bias term $M_2\,\mathrm{d}\Omega$ may differ from patch to patch. When the volume estimation is applied to an erf-clipped constant gradient edge, edgeheight is replaced by cliprange and h by $h_{\text{clip}} \equiv \text{clip}_{\text{erf}}(ar + b)$ and we can calculate M_2

$$\left|\frac{\mathrm{d}}{\mathrm{d}r} h_{\text{clip}}(r)\right| = a \exp\left(-\frac{\pi(ar + b - t)^2}{\text{cliprange}^2}\right) \qquad (29)$$

$$\begin{aligned}
M_2 &= \frac{1}{\text{cliprange}} \int_{\substack{\text{edge}\\ \text{thickness}}} \frac{\mathrm{d}h_{\text{clip}}}{\mathrm{d}r} r^2\,\mathrm{d}r \approx \frac{a}{\text{cliprange}} \int_{-\infty}^{\infty} r^2 \\
&\quad \times \exp\left(-\frac{\pi(ar + b - t)^2}{\text{cliprange}^2}\right)\mathrm{d}r \\
&= \frac{\text{cliprange}^2}{2\pi a^2} \equiv w^2. \qquad (30)
\end{aligned}$$

The gradient a may differ from patch to patch. The total area bias due to $M_2\,\mathrm{d}\Omega$ is

$$\frac{\text{cliprange}^2}{2\pi} \int_{\text{all patches}} \frac{1}{a^2}\,\mathrm{d}\Omega \qquad (31)$$

and can be extrapolated from two measurements with different cliprange values.

8.2. Displacement of curved step edge by a 3D Gaussian filter

The displacement of an erf-clipped constant gradient edge caused by a Gaussian filter of size σ can be calculated as follows. A 3D constant gradient edge with local curvatures $1/R_1$ and $1/R_2$ can be modelled $(X, y, z \ll |R_1|, |R_2|)$ as $h(r) = ar + b$ with

$$r = \sqrt{X^2 + X(y^2/R_1 + z^2/R_2)}$$

and

$$X \equiv x - x_{r=0}.$$

The gradient is then indeed of constant magnitude

$$\begin{aligned}
&\frac{|\text{grad}(h(r))|^2}{a^2} \\
&\quad = 1 + \frac{(y^2/2R_1 + z^2/2R_2)^2 + (yX/R_1 + zX/R_2)^2}{X^2 + y^2X/R_1 + z^2X/R_2} \\
&\quad = 1 + O\left[\left(\frac{X, y, z}{|R_1|, |R_2|}\right)^2\right]. \qquad (32)
\end{aligned}$$

Along the same lines as in 2D the smoothing of the |gradient| of the erf-clipped edge

$$\left|\frac{\mathrm{d}}{\mathrm{d}r} h_{\mathrm{clip}}(r)\right| = a \exp\left(-\frac{r^2}{2w^2}\right) \tag{33}$$

first goes along the tangential dimensions y and z

$$\begin{aligned}\frac{1}{2\pi\sigma^2}\exp\left(-\frac{y^2+z^2}{2\sigma^2}\right) * \left|\frac{\mathrm{d}}{\mathrm{d}r} h_{\mathrm{clip}}(r)\right|_{y,z=0} \\ \approx a \exp\left(-\frac{X^2}{2w^2}\right) F_y\left(\frac{X}{R_1}\right) F_z\left(\frac{X}{R_2}\right) \\ \approx a \exp\left(-\frac{\left(X+\frac{\sigma^2}{2R_1}+\frac{\sigma^2}{2R_2}\right)^2}{2w^2}\right)\end{aligned} \tag{34}$$

where the functions F_y and F_z are defined as in section 6 (cf (26)). Note that tangential smoothing displaces the edge by $-(\sigma^2/2R_1 + \sigma^2/2R_2)$.

Next we perform the (radial) x-smoothing

$$\begin{aligned}\left|\frac{\mathrm{d}}{\mathrm{d}r} h_{\mathrm{clip}}(r)\right|_{\mathrm{smoothed}} \approx \frac{1}{\sqrt{2\pi}\sigma}\exp\left(-\frac{X^2}{2\sigma^2}\right) \\ * a \exp\left(-\frac{\left(X+\frac{\sigma^2}{2R_1}+\frac{\sigma^2}{2R_2}\right)^2}{2w^2}\right)\Bigg|_{X=r} \\ \frac{aw}{\sqrt{\sigma^2+w^2}}\exp\left(-\frac{\left(r+\frac{\sigma^2}{2R_1}+\frac{\sigma^2}{2R_2}\right)^2}{2(\sigma^2+w^2)}\right)\end{aligned} \tag{35}$$

for $\sigma < 2\sqrt{w \min[R_1, R_2]}$.

Also in 3D the Gaussian shape of $|\mathrm{d}/\mathrm{d}r\, h_{\mathrm{clip}}(r)|$ and the erf character of $h_{\mathrm{clip}}(r)$ are largely preserved by Gaussian smoothing.

Area bias due to displacement. The displacement of an erf-clipped constant gradient edge caused by a Gaussian filter of size σ is $-(\sigma^2/2R_1 + \sigma^2/2R_2)$ and results in an area bias contribution

$$-\frac{\sigma^2}{2}\int_{\text{all patches}}\left(\frac{1}{R_1}+\frac{1}{R_2}\right)(R_1+R_2)\,\mathrm{d}\Omega. \tag{36}$$

For each sphere this bias contribution is $-8\pi\sigma^2$. For other objects the bias is shape dependent and larger. For area measurement based on the Laplacian-of-Gaussian ($\sigma \approx \sigma_{\mathrm{preclip}}$) this bias is compensated.

In 3D a second—shape independent—bias due to edge thickening occurs which cannot be compensated (see section 8.3).

Just as in 2D, for $\sigma \approx \sigma_{\mathrm{preclip}}$ the offset of the Laplacian-of-Gaussian zerocrossing position can also be corrected by erf-clipping and appropriate Gaussian smoothing (without built-in gradient).

8.3. Edge thickening bias of surface area due to 3D Gaussian smoothing

Due to Gaussian smoothing the slope

$$\left|\frac{\mathrm{d}}{\mathrm{d}r} h_{\mathrm{clip}}(r)\right| = a \exp\left(-\frac{r^2}{2w^2}\right) \tag{37}$$

is replaced by

$$\begin{aligned}\left|\frac{\mathrm{d}}{\mathrm{d}r} h_{\mathrm{clip}}(r)\right|_{\mathrm{smoothed}} \approx \frac{aw}{\sqrt{\sigma^2+w^2}} \\ \times \exp\left(-\frac{(r+\sigma^2/2R_1+\sigma^2/2R_2)^2}{2(\sigma^2+w^2)}\right).\end{aligned} \tag{38}$$

Therefore the second moment of $r(h_{\mathrm{clip}})$, $M_2 = w^2$ becomes $M_2|_{\mathrm{smoothed}} = w^2 + \sigma^2$.

The patch area bias due to smoothing is thus $\sigma^2\,\mathrm{d}\Omega$. For each object without tunnels or enclosed cavities the solid angles $\mathrm{d}\Omega$ add up to 4π and smoothing leads to a constant total-area bias of $4\pi\sigma^2$.

9. Methods

In the preceding sections we have introduced a method for measuring the edge length/surface area of an isophote or a zerocrossing. Being aware of the edge displacement (sections 6 and 8.2), we consider the simple method that measures the length of an isophote at level t. The digital implementation can be achieved using two different strategies.

9.1. Strategies

In the first strategy, we start with clipping around a certain 'threshold' to ensure a constant edge height. The result of clipping is then shifted perpendicularly to the edge according to (6) and (7). Subtraction of the two shifted edges cancels the contribution of the SDGD. As a consequence the size of the displacement (fsize) becomes irrelevant as well. Following (3), the edge length is given by

$$\text{edgelength} = \text{volumeof}(|\text{grad}(\text{clip}_{\text{erf}}(\text{ori}))|)/\text{cliprange}. \tag{39}$$

Note that clipping is the only operation left that increases the bandwidth of the original image by a factor of edgeheight/cliprange (cf (11)).

The second strategy starts with shifting the edge image over a carefully selected distance fsize, selecting a suitable 'threshold' level and applying the clipping around the selected 'threshold' to both shifted versions. Subtracting the two versions produces a bar whose volume is proportional to the edge length. According to (3) the

measured edge length is given by

$$\text{edgelength} = \frac{1}{\text{fsize} \cdot \text{clip}_{\text{range}}} \text{volumeof}$$
$$\times \left(\text{clip}_{\text{erf}} \left(\text{ori} + \frac{\text{fsize}}{2} |\text{grad(ori)}| + \frac{\text{fsize}^2}{8} \text{SDGD(ori)} \right) \right.$$
$$\left. - \text{clip}_{\text{erf}} \left(\text{ori} - \frac{\text{fsize}}{2} |\text{grad(ori)}| + \frac{\text{fsize}^2}{8} \text{SDGD(ori)} \right) \right). \quad (40)$$

The filters used to build |grad| and SDGD are the first and second derivatives of a Gaussian. In order to guarantee isotropy, all partial derivatives used to construct the SDGD must have the same built-in low-pass filter, equal to σ. At the same time this σ is used to avoid spurious aliasing.

The first strategy allows us to choose the following parameters:

(a) the isophote level t and clipping range (cliprange/edgeheight);
(b) the built-in σ of the derivative filters.

The second strategy has one additional parameter:

(c) the size of the analogue max and min filters (fsize)

Strategy 1 is independent of max-min filter size to create a constant edge width. Its results must equal theoretical predictions in the limit of fsize $\to 0$. Consequently, in 3D, one bias term, (fsize^2/12) dΩ, does not occur (cf (28))

$$\int_{\text{patch}} |\text{grad } h| \text{d}x \, \text{d}y \, \text{d}z$$
$$= \int_{r_{\min}}^{r_{\max}} |\text{grad } h|(R_1 + r)(R_2 + r) \, \text{d}r \, \text{d}\Omega$$
$$= \text{edgeheight}(R_1 R_2 + M_2) \, \text{d}\Omega.$$

Strategy 2 is far more complex than strategy 1 without producing better results (Verbeek and van Vliet 1992). From now on we will consider only strategy 1.

9.2. Isophote (GC) and zerocrossing (GCL) length/area

The erf-clipping can be applied to the sampled image (pseudo-threshold method, GC, gradient-clip) or to the output of the Laplacian-of-Gaussian (zerocrossing method, GCL, gradient-clip-Laplace). Figures 3 and 4 illustrate both methods by showing the edge shape, the edge position, and the slope at the edge position after all steps. In the first method the isophote selected in the experiment is at half the edge height while in the second method it is the zero-isophote. We have set the clip range to $\frac{1}{4}$ of the edge height or second derivative range. The built-in σ of the gradient filter can be set to any value ($\sigma < 2R$) for the first method while in the second method it depends on the width of the optical point spread function (approximated by a Gaussian σ_{PSF} (Verbeek and van Vliet 1991)) and the width of the Laplacian-of-Gaussian, σ_{Laplace}. To guarantee that the edge position is restored experiments showed that $\sigma \approx 1.01\ \sigma_{\text{preclip}}$ yields an unbiased edge position. From section 7 it follows that the 2D GCL edge length estimator yields unbiased results. In 3D, both surface area estimators (GC and GCL) are biased. We summarize as follows:

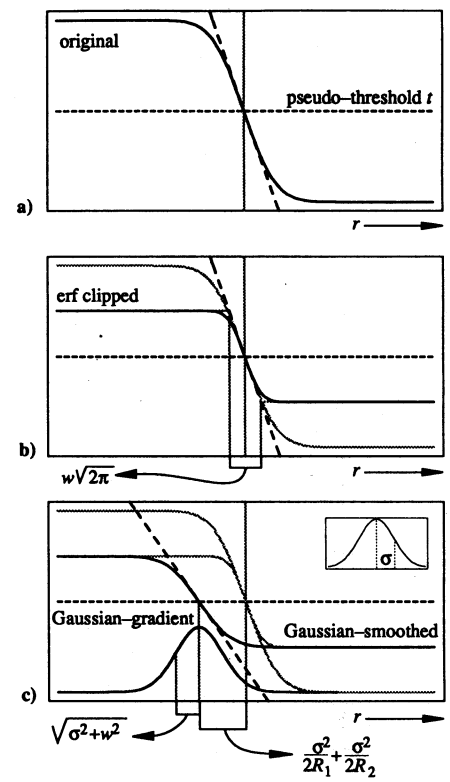

Figure 3. Various stages of the GC method applied to a curved edge: (*a*) original bandlimited edge; (*b*) constant height edge after erf-clipping; (*c*) Gaussian smoothing displaces the edge towards the centre of the osculating circle. Consequently, the GC method yields a negative bias.

Bias of isophote area. The bias of surface area measurements with the GC method due to 3D Gaussian smoothing is shape dependent. There are three contributions to the measured bias:

(a) shift of half height edge location (cf (36)) (negative);
(b) w^2 (positive) and
(c) σ^2 (positive).

w^2 originates from the edge slope and σ^2 is due to the

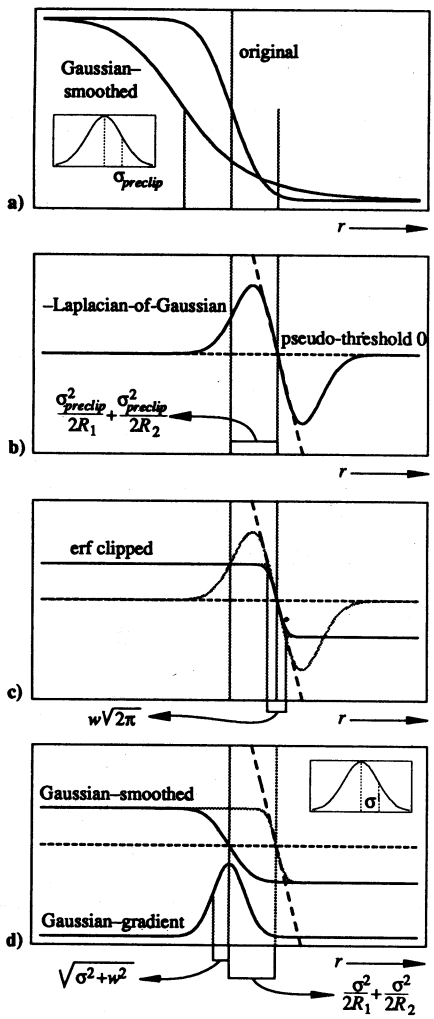

Figure 4. Various stages of the GCL method applied to a curved edge: (*a*) original bandlimited edge and a Gaussian smoothed version; (*b*) Laplacian-of-Gaussian displaces the edge away from the centre of the osculating circle; (*c*) constant height edge after erf-clipping. Erf-clipping is applied only to the sloped region of the edge. The resulting clipping levels ($clip_{high}$ and $clip_{low}$) are propagated to fill the interior and the exterior of the object; (*d*) Gaussian smoothing displaces the edge towards the centre of the osculating circle. Choosing $\sigma_{gradient}$ equal to $\sigma_{preclip}$ yields the correct edge location. Consequently, the Gaussian-gradient is centred around the original edge position.

Gaussian low-pass filter built-in the gradient filter. The theoretical bias for spheres is (cf (36), (12), (25*a*) and section 8.3):

$$\begin{aligned}\text{bias} &= -8\pi(\sigma_{PSF}^2+\sigma^2)+4\pi w^2+4\pi\sigma^2\\ &= -4\pi\sigma^2-4\pi\left(2-\frac{\text{cliprange}^2}{\text{edgeheight}^2}\right)\sigma_{PSF}^2. \qquad (41)\end{aligned}$$

Bias of zerocrossing area. The bias of surface area measurements with the GCL method due to 3D Gaussian smoothing is independent of the object shape. There are two contributions to the measured bias given an exact edge location:

(a) w^2 (positive) and
(b) σ^2 (positive).

The w^2-contribution originates from the original edge slope. Given a physical step edge we have $w(\sigma_{preclip}) = 1/\pi f_{maxerf}(\sigma_{preclip})$ as given in (12); for a physical edge resembling a step edge smoothed with σ_{slope} we get $w(\sqrt{\sigma^2_{slope}+\sigma^2_{preclip}})$. In practice σ_{slope} may vary over the surface, say between 0 and $3\sigma_{PSF}$.

The σ^2-contribution is due to the Gaussian low-pass filter built-in the gradient filter. (Sampling at the Nyquist rate (1N) corresponds to $\sigma_{PSF} = 0.9$.)

10. Experiments

Experiments are necessary to test the presented theory, the robustness, and the applicability of it.

10.1. Test images

The test images contain a simulated image of a step edge object imaged through an optical system and sampled at the Nyquist frequency (1N) or at 2 times the Nyquist frequency (2N). Randomly positioned bandlimited disc/sphere/ellipsoid images are constructed as test objects. To construct an arbitrary bandlimited object, we start out from its Fourier transform, ensure proper bandlimitation by multiplying with the perfect in-focus OTF (optical transfer function) (Born and Wolf 1959, Williams and Becklund 1989), and apply an inverse Fourier transform to obtain the desired image. In 3D the OTF is replaced by an anisotropic Gaussian function that shows the same behaviour as the corresponding OTF (Verbeek and van Vliet 1991). Using a compensating anisotropic Gaussian for the derivative filters we can obtain an isotropic $\sigma_{preclip}$.

The true surface area of 3D ellipsoids was computed numerically with *Mathematica* (Wolfram 1988) based upon theory from 'Differential Geometry' (Boehm 1990). In earlier work we found that the 2D point spread function of an in-focus optical system is well described by a 2D Gaussian; $\sigma_{PSF} = 0.9$ (van Vliet and Verbeek 1991, Verbeek and van Vliet 1991).

10.2. Isophote and zerocrossing length of 2D discs

Both variants (GC and GCL) of our edge length estimator were tested. The results are shown in figure 5. Sampling at 2N roughly complies with condition (13). Note that sampling at 1N gives a larger CV but still of the order of the bias and thus is found to be sufficient in practice. The GC method shows the expected bias due

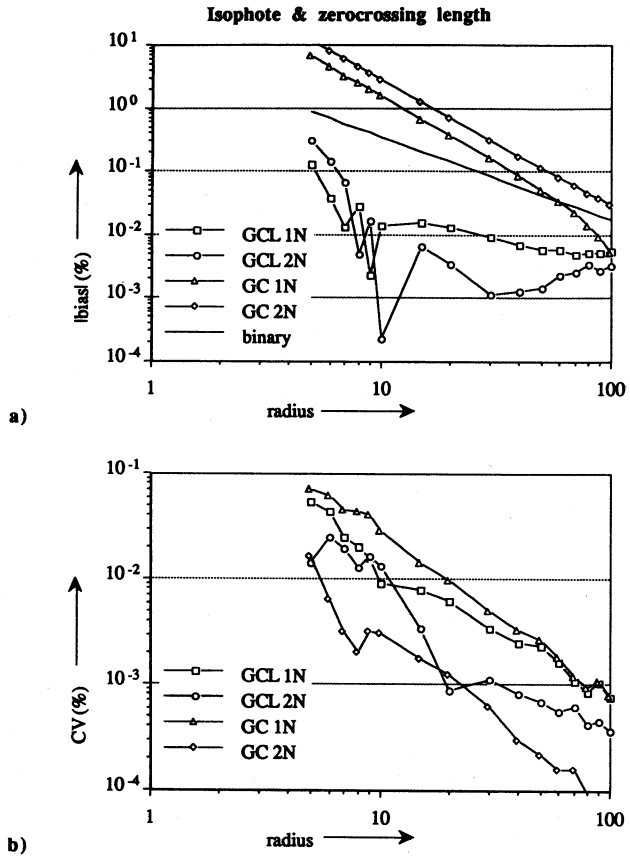

Figure 5. For each sample point in these figures 25 randomly positioned bandlimited 2D discs were generated. The performance of two variants of our edge length estimator ($\sigma_{Laplace} = 1.5$) applied to discs of different bandlimitation (1N and 2N) is compared with the best classical technique available (Young 1988). (*a*) The absolute relative error (in %) for the perimeter length. (*b*) The CV (in %) for the perimeter length.

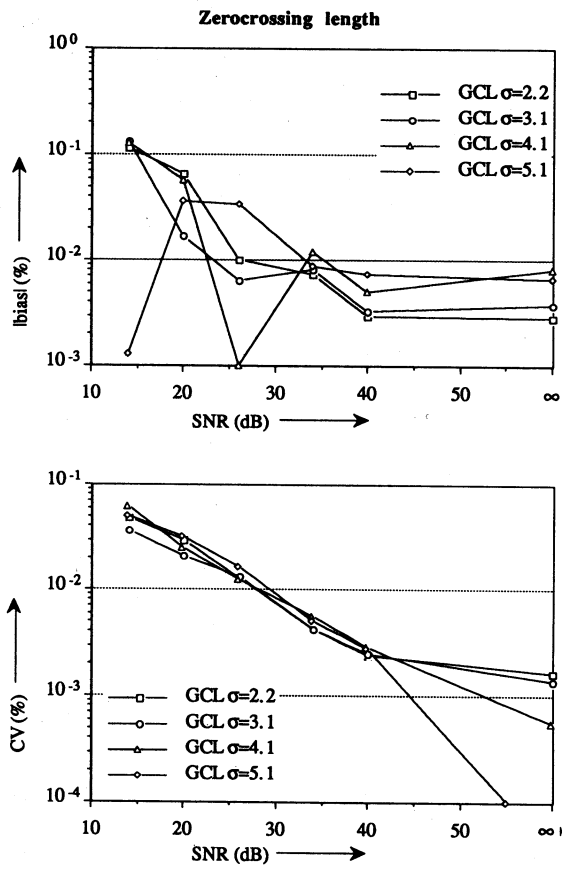

Figure 6. For each sample point in these figures 25 randomly positioned bandlimited 2D discs were generated. The images were disturbed by various amounts of additive Gaussian noise. The robustness of our edge length estimator for different σ's on a bandlimited (1N) sampled disc of radius 20 is shown. (*a*) The absolute relative error (in %) for the perimeter length. (*b*) The CV (in %) for the perimeter length.

to edge displacement by σ smoothing. Comparing figure 5 with the results reported for discs by Young (1988) we notice: (i) when using GCL our bias for discs is an order of magnitude smaller; (ii) our CV's for both 1N and 2N discs are one order of magnitude smaller than the ones reported by Young (1988).

10.3. Robustness of perimeter length in the presence of noise

To test the robustness of our GCL technique in the presence of noise we added various amounts of independent Gaussian distributed noise to a disc of radius 20. The SNR is defined as

$$\mathrm{SNR(dB)} = 20 \log\left(\frac{\text{edgeheight}}{\sigma_{noise}}\right).$$

The $\sigma_{Laplace}$ reduces the noise without dramatic changes in performance of the edge position and therefore the length estimator (cf figure 6). For SNR's larger than 30 dB the method performs similarly as in the noise free case. The CVs are still decreasing—especially for larger $\sigma_{Laplace}$. In 3D, filters with the same $\sigma_{Laplace}$ can successfully be applied to much lower SNR's. Thanks to $\sigma_{Laplace}$, sampling at 1N complies with condition (13).

10.4. Zerocrossing position of curved edges in 2D and 3D

Section 7 concludes that applying erf-clipping and Gaussian smoothing *without gradient* to the result of Laplacian-of-Gaussian edge detection will correct the zerocrossing position. We only show a 3D example (cf figure 7) because the behaviour in 2D is exactly the same. Figure 7 shows no difference in performance between spheres and ellipsoids. Sampling at 2N roughly complies with condition (13). Note that sampling at 1N shows the same CV and even a slightly smaller bias for small radii. The bias in edge position is an order of magnitude smaller than the bias of the Gaussian-of-Laplacian edge detector over almost the entire range of radii.

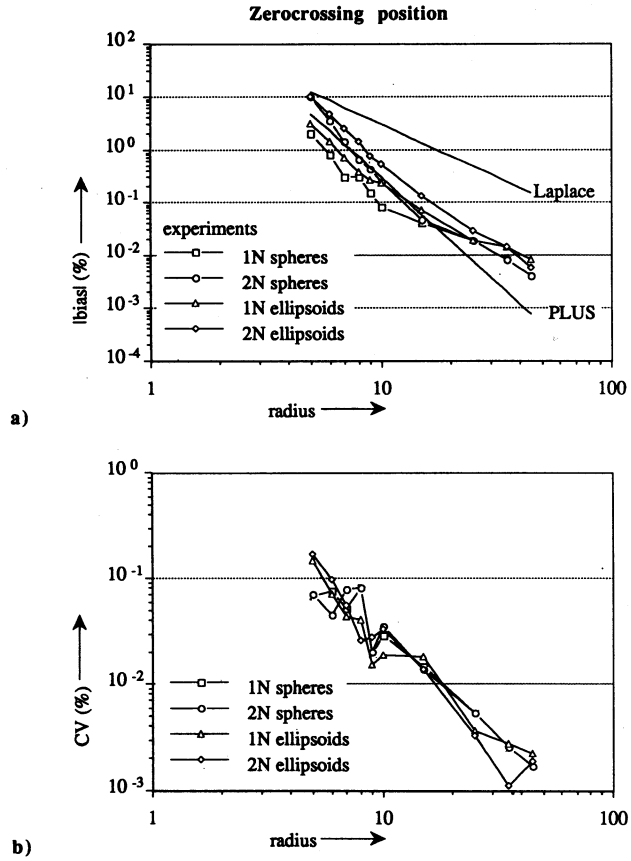

Figure 7. For each sample point in these figures 10 randomly positioned bandlimited 3D spheres or ellipsoids were generated. The relative error in zerocrossing position is presented for spheres and ellipsoids of different bandlimitation (1N and 2N). The values can be compared with results from earlier work (van Vliet and Verbeek 1991; Verbeek and van Vliet 1991). Laplace requires and has got 1N, PLUS requires 3N, but has got 2N sampling. (*a*) The absolute relative error (in %) for the zerocrossing position. (*b*) The CV (in %) for the measured zerocrossing position.

10.5. Isophote area (GC) for 3D spheres and ellipsoids

From (36) one can derive that as in 2D the surface area of the isophote at half edge height produces a biased estimate. Unlike in 2D the 3D bias is constant. It only depends on the object shape. Table 2 confirms this theory. Both spheres and ellipsoids have a constant bias over the entire range of object size. Figure 8 shows the performance of the GC surface area estimator before and after subtraction of the theoretical bias. For convex non-spherical shapes the correction is partial. The correction gives an enormous reduction in bias: almost two orders of magnitude for spheres and at least one order of magnitude for our ellipsoids. The CV's for spheres and ellipsoids are the same. Sampling at 2N roughly complies with condition (13). Note that sampling at 1N gives large CV's but still of the order of the bias

Table 2. Bias of surface area measurements due to 3D Gaussian smoothing for the GC method. Three phenomena contribute to the measured bias: shift of half height edge location cf (36) (negative), w^2 (positive) and σ^2 (positive). w^2 originates from the edge slope and σ^2 is due to the Gaussian low-pass filter built in the gradient filter. Theoretical bias for spheres is (cf (41)): bias $= -8\pi(\sigma_{PSF}^2 + \sigma^2) + 4\pi w^2 + 4\pi\sigma^2 = -4\pi\sigma^2 - 4\pi(2 - (\text{cliprange/edgeheight})^2)\sigma_{PSF}^2$.

			Theory	Experiment	
σ_{PSF}	σ	cliprange / edgeheight	Bias spheres	Bias spheres R $R \in (5\text{–}45)$	Bias ellipsoids (0.8R, 1.0R, 1.2R) $R \in (5\text{–}45)$
0.9	1.5	0.25	−48.0	−48.8	−54.5
1.8	1.5	0.25	−107	−108	−117

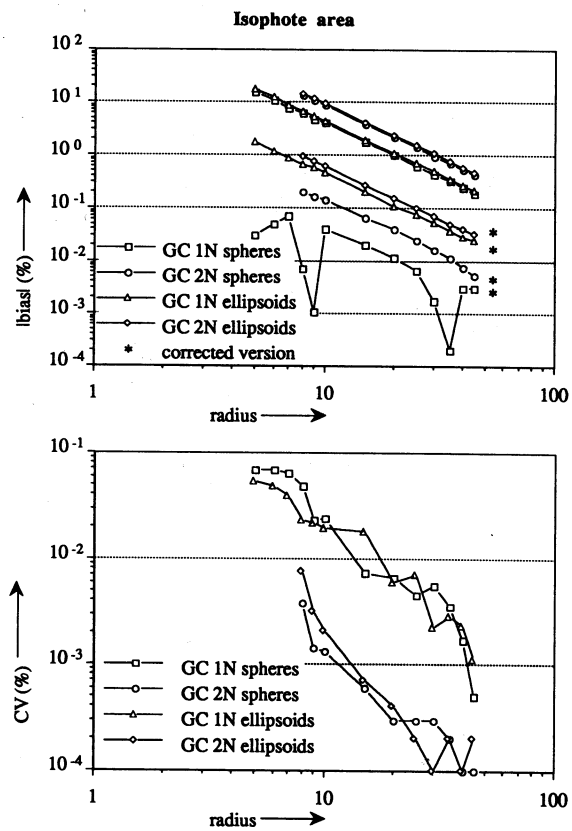

Figure 8. For each sample point in these figures 10 randomly positioned bandlimited 3D spheres or ellipsoids were generated. The performance of a simple version of our surface area estimator ($\sigma = 1.5$) is shown for spheres and ellipsoids of different bandlimitation (1N and 2N). We measure the surface area of the isophote at half edge height. The resulting bias is independent of the size but dependent on the shape of the object. For spheres sampled at 1N ($\sigma = 1.5$) the bias equals −48.0 and for spheres sampled at 2N ($\sigma = 1.5$) the bias equals −107. (*a*) The absolute relative error (in %) for the measured surface area before and after (*) subtraction of the theoretical bias for spheres. (*b*) The CV (in %) for the measured surface area.

Table 3. Bias of surface area measurements due to 3D Gaussian smoothing for the GCL method. Two phenomena contribute to the measured bias given an exact edge location: w^2 and σ^2. The w^2-contribution originates from the original edge slope. Given a physical step edge we have $w(\sigma_{\text{preclip}}) = 1/\pi f_{\text{maxerf}}(\sigma_{\text{preclip}})$ as given in (12); for a physical edge resembling a step edge smoothed with σ_{slope} we get $w(\sqrt{(\sigma^2_{\text{slope}} + \sigma^2_{\text{preclip}})})$. In practice σ_{slope} may vary over the surface, say between 0 and $3\sigma_{\text{PSF}}$. The σ^2-contribution is due to Gaussian low-pass filter built-in the gradient filter.
(Sampling at 1N corresponds to $\sigma_{\text{PSF}} = 0.9$.)

				Theory			Experiment	
σ_{PSF}	σ_{preclip}	f(cliprange, secderrange)	$\frac{\text{cliprange}}{a}$	w^2	σ^2	$4\pi(w^2 + \sigma^2)$	Spheres R $R \in (40, 45)$	Ellipsoids $R(0.8, 1, 1.2)$ $R \in (40, 45)$
0.9	1.75	0.25	0.53	0.044–0.15	3.12	39.6–40.9	40.2†	40.5†
0.9	2.20	0.25	0.67	0.070–0.18	4.91	62.3–63.6	63.5†	63.8†
0.9	3.13	0.25	0.95	0.14–0.25	10.0	127–129	130	131
0.9	4.10	0.25	1.24	0.25–0.35	17.1	218–220	227	231
1.8	2.34	0.25	0.71	0.080–0.19	5.60	70.5–71.8	72.4†	73.2†

† $R \in 20, 25, 30, 35, 40, 45$).

and thus is found to be sufficient in practice. Comparing figure 8 with the results reported for spheres by (Mullikin and Verbeek 1993) we notice: (i) our bias for spheres is one order of magnitude smaller; (ii) our CV's for spheres sampled at 1N and 2N are respectively two and three orders of magnitude smaller.

10.6. Zerocrossing area (GCL) for 3D spheres and ellipsoids

Section 8.3 predicts a bias per surface patch of $(w^2 + \sigma^2)\,d\Omega$. The bias due to the edge shape after erf-clipping is $w^2\,d\Omega$, whereas 3D Gaussian smoothing contributes the second term $\sigma^2\,d\Omega$. Table 3 shows the calculation of the predicted bias and empirical results. For small radii the empirically obtained bias is somewhat larger than the theoretical prediction. Figure 9 shows the performance of GCL before and after subtraction of the theoretical bias. Sampling at 2N roughly complies with condition (13). Note that sampling at 1N is found to be sufficient in practice. Comparing figure 8 with the results reported for spheres by (Mullikin and Verbeek 1993) we notice: (i) our bias for small radii (<10) is the same, but for large radii ($\geqslant 25$) our bias is at least one order of magnitude smaller; (ii) our CV's for both 1N and 2N spheres are one order of magnitude smaller for small radii (<10) and two orders of magnitude smaller for large radii ($\geqslant 25$).

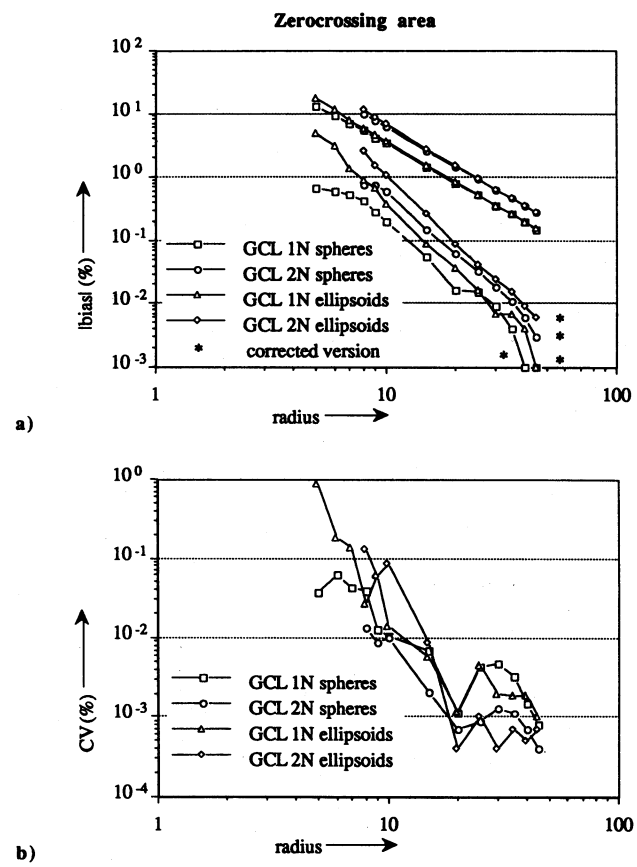

Figure 9. For each sample point in these figures 10 randomly positioned bandlimited 3D spheres or ellipsoids were generated. The performance of our zerocrossing surface area estimator ($\sigma_{\text{Laplace}} = 1.5$) before and after subtraction of the *predicted* constant bias term are compared for spheres and ellipsoids of different bandlimitation (1N and 2N). For 1N images and $\sigma \approx \sigma_{\text{preclip}} = 1.75$ the bias equals 39.6 and for 2N images and $\sigma \approx \sigma_{\text{preclip}} = 2.25$ the bias equals 70.5. (*a*) The absolute relative error (in %) for the measured surface area before and after (*) subtraction of the theoretical bias. (*b*) The CV (in %) for the measured surface area.

11. Conclusions

In this paper we estimate 2D edge length and 3D surface area through grey-volume measurements. The method is not empirical but, apart from a few plausible assumptions,

based on sampling theory. The volume of a grey value landscape is directly proportional to the sum of the samples for all images sampled at half the Nyquist rate or higher. An edge is transformed into volume by giving it a constant height after which the edge is shifted perpendicularly to the edge over a small distance. The constant height obtained by 'erf-clipping' in the linear region of the edge. The edge location defined via the clipping levels is shading-dependent (GC method). For a constant and isotropic shift of the edge we apply a Taylor series expansion along the gradient direction. The derivative-of-Gaussian filters used are sampling invariant and allow shifts in the subpixel region. However, for curved edges the built-in Gaussian introduces a systematic edge displacement towards the centre of the osculating circle.

To use a more appropriate edge definition that does not suffer from shading, the erf-clipping is applied to the output of a Laplacian-of-Gaussian filter (GCL method). The choice of the Laplacian-of-Gaussian offers a *compensating* systematic edge displacement (away from the centre of the osculating circle) and hence an unbiased estimate of 2D edge length and position. (For position estimation clipping is only followed by a Gaussian filtering.) This works for all edges with a radius larger than the support of the built-in Gaussian filter.

Extension to higher dimensionality is straightforward but leads to biased (hyper-)area estimations (the edge position remains unbiased). For 3D objects without tunnels or enclosed cavities the surface area bias amounts to a constant correction per object and an unbiased estimator can still be constructed.

Our method can be implemented using simple derivatives-of-Gaussian filters and non-linear image scaling (erf-clipping). The algorithm is of the same complexity as the Laplacian-of-Gaussian filter followed by thresholding that produces the binary images for the traditional methods. The edge position of curved edges in our methods is much better preserved than by Laplacian-of-Gaussian filtering.

Experiments show that unbiased estimators for 2D edge length and 3D surface area can be constructed. Comparing our method with existing binary methods (Young 1988, Mullikin and Verbeek 1993) we notice that: (i) our bias is almost everywhere an order of magnitude smaller; (ii) our CV's in 2D are more than an order of magnitude smaller and our CV's in 3D are two or three orders of magnitude smaller. We may conclude that proper sampling really pays off. Moreover, our method easily takes care of edge shifts by optical smoothing (σ_{PSF}).

The experiments also show that some undersampling does not sacrifice the performance of our method. Sampling at the Nyquist rate, derivative-of-Gaussian with $\sigma = 1.5$ (GC) or sampling at the Nyquist rate, Laplacian-of-Gaussian with $\sigma_{Laplace} = 1.5$ and derivative-of-Gaussian with $\sigma = 1.75$ (GCL) performs well.

Acknowledgments

This work was partially supported by the Dutch Government as part of the SPIN-FLAIR II program 'Delft Intelligent Assembly Cell', the SPIN-3D program for 3D biomedical image analysis and by the Netherlands Foundation for Biomedical Research NWO-MEDIGON, grant 900-538-016.

13. References

Berzins V 1984 Accuracy of Laplacian edge detectors *Computer Vision, Graphics Image Process.* **27** 195–210

Boehm W 1990 Differential Geometry II *Curves and Surfaces for Computer Aided Geometric Design: A Practical Guide* (New York: Academic) pp 267–83

Born M and Wolf E 1959 *Principles of Optics, sixth edition* Pergamon

Dorst L 1986 Discrete straight lines: parameters, primitives and properties *PhD Thesis* Delft University of Technology

Dorst L and Smeulders A W M 1986 'Best linear unbiased estimator for properties of digitized straight lines. *IEEE Trans. Pattern Analysis and Machine Intelligence PAMI-8* 276–82

—— 1987 Length estimators for digitized contours. *Computer Vision, Graphics Image Process.* **40** 311–33

Eberly D and Lancaster J 1991 On gray scale image measurements I: arc length and area *CVGIP: Graphical Models Image Process.* **53** 538–49

Eberly D, Lancaster J and Alyassin A 1991 On gray scale image measurements II: surface area and volume. *CVGIP: Graphical Models and Image Processing* **53** 550–62

Ellis T J and Proffitt D 1979 Measurement of the length of digitized curved lines. *Computer Graphics Image Process.* **10** 333–47

Freeman H 1970 Boundary encoding and processing *Picture Processing and Psychopictorics* (New York: Academic) pp 241–66

Gesbert S, Howard C V, Jeulin D and Meyer F 1990 The use of basic morphological operations for 3D biological image analysis *Transactions of the Royal Microscopy Society* (Bristol: Hilger) pp 293–6

Groen F C A and Verbeek P W 1978 Freeman code probabilities of object boundary quantized contours. *Computer Graphics Image Process.* **7** 391–402

Hahn U and Sandau K 1989 Precision of surface area estimation using spatial grids. *Acta Stereology* **8** 425–30

Howard V C and Sandau K 1992 Measuring the surface area of a cell by the method of the spatial grid with a CSLM: a demonstration *J. Microsc.* **165** 183–8.

Kulpa Z 1977 Area and perimeter measurement of blobs in discrete binary pictures *Computer Graphics Image Process.* **6** 434–54

Meyer F 1992 Mathematical morphology: from two dimensions to three dimensions *J. Microsc.* **156** 5–28

Mullikin J C 1992 Boundary description and measurement with sub-pixel/voxel accuracy *11th IAPR Int. Conf. Pattern Recognition (The Hague)* (IEEE)

Mullikin J C and Verbeek P W 1993 Surface area estimation of digitized planes *Bioimaging* **1** 6–16

Proffitt D and Rosen D 1979 Metrication errors and coding efficiency of chain-encoding schemes for the representation of lines of finite length *Computer Graphics Image Process* **10** 318–22

van Vliet L J and Verbeek P W 1991 On the location error of curved edges in low-pass filtered 2D and 3D images II: application aspects *Internal report*

Verbeek P W 1985 A class of sampling-error free measures in oversampled band-limited images. *Pattern Recognition Lett.* **3** 287–92

Verbeek P W and van Vliet L J 1991 On the location error of curved edges in low-pass filtered 2D and 3D images I: theory *Internal Report*

—— 1992 An estimator of edge length and surface area in digitized 2D and 3D images. 11th IAPR *Int. Conf. Pattern Recognition* (*The Hague*) (IEEE)

Verbeek P W, Vrooman H A and van Vliet L J 1988 Low level image processing by max–min filters *Signal Process.* **15** 249–58

Vossepoel A M and Smeulders A W M 1982 Vector code probabilities and metrication error in the representation of straight lines of finite length *Computer Graphics Image Process.* **20** 347–64

Williams C S and Becklund O A 1989 *Introdction to the Optical Transfer Function* (New York: Wiley)

Wolfram S 1988 *Mathematica, second edition* (Redwood City, CA: Addison-Wesley)

Young I T 1988 Sampling density and quantitative microscopy *Anal. Quant. Cytol. Histol.* **10**(4) 269–75